Available online at www.sciencedirect.com
ScienceDirect
Trans. Nonferrous Met. Soc. China 35(2025) 2726−2733
Transactions of Nonferrous Metals Society of China
www.tnmsc.cn

HeLa cell cytotoxicity of K−Na co-doped layered-MnO_2

Qin CHEN, Jin-quan YANG, Jue LIU

Hunan Provincial Maternal and Child Health Care Hospital, Changsha 410008, China

Received 17 January 2025; accepted 10 May 2025

Abstract: K−Na co-doped δ-MnO_2 (KNMOH) nanoflowers were synthesized, and their cytotoxic effects against HeLa cervical cancer cells were evaluated. The KNMOH exhibited significant dose- and time-dependent cytotoxicity at concentrations of 50 and 100 μg/mL. After 24 h of incubation treatment, cell viability decreased to (36.8±6.5)% and (33.4±6.4)% at 50 and 100 μg/mL, respectively. With extended exposure to 48 h, cell viability was (45.2±2.3)% and (32.3±2.8)% at the same concentrations. Phase-contrast microscopy revealed characteristic morphological changes including cell shrinkage and membrane blebbing formation, indicative of cell death. These findings demonstrate the potential of KNMOH nanoflowers as a cytotoxic agent for cervical cancer applications and provide a foundation for further mechanistic studies.

Key words: K−Na co-doped δ-MnO_2; cytotoxicity; HeLa cells; interlayer spacing; cervical cancer

1 Introduction

Cancer remains a paramount global health challenge, necessitating the continuous development of innovative and effective therapeutic strategies to overcome the limitations of conventional treatments, such as non-specific cytotoxicity, severe side effects, and the emergence of drug resistance [1,2]. Nanomaterials have emerged as a promising frontier in oncology, offering unique physicochemical properties that can be harnessed for targeted drug delivery, enhanced imaging, and novel therapeutic modalities [3,4]. Among the diverse classes of nanomaterials, transition metal oxides, particularly manganese dioxide (MnO_2), have garnered significant attention due to their inherent biocompatibility at physiological concentrations, tunable properties, and versatile functionalities [5−7].

MnO_2 nanomaterials have recently emerged as promising candidates for biomedical applications due to their unique physicochemical properties and biocompatibility [8,9]. Studies have demonstrated that MnO_2 nanoparticles can interact with cancer cells and exhibit cytotoxic effects through various mechanisms including reactive oxygen species (ROS) generation and cellular membrane disruption [10]. FAN et al [11] reported that MnO_2 nanoparticles could effectively kill cancer cells by depleting glutathione and generating oxygen. Similarly, LIN et al [12] demonstrated that MnO_2-based nanomaterials showed excellent tumor suppression effects in vivo.

The structural modification of MnO_2 through alkali metal doping has been shown to alter its surface properties and potentially enhance its biological activity [13]. Among various polymorphs, the layered δ-MnO_2 structure with intercalated cations offers expanded interlayer spacing and enhanced stability [14]. However, the cytotoxic effects of K−Na co-doped δ-MnO_2 against cervical cancer cells have not been systematically investigated.

Corresponding author: Qin CHEN, Tel: +86-18670720360, E-mail: 312961631@qq.com
https://doi.org/10.1016/S1003-6326(25)66843-9

HeLa cells, derived from human cervical adenocarcinoma, have been widely used as a model system for cancer research due to their well-characterized properties and response to various treatments [15]. The evaluation of novel materials' cytotoxicity using HeLa cells provides valuable insights into their potential therapeutic applications.

Therefore, this study aims to synthesize K−Na co-doped δ-MnO_2 (KNMOH) nanoflowers and systematically evaluate their cytotoxic effects against HeLa cervical cancer cells. The dose-response relationship and time-dependent effects were investigated to provide fundamental data for potential therapeutic applications.

2 Experimental

2.1 Materials and reagents

The main reagents used in this study included HeLa cells (human cervical cancer cells), purchased from Wuhan Pusaite Biotechnology Co., Ltd., China. Dulbecco's modified eagle medium (DMEM, Lot No. 6124448) and fetal bovine serum (FBS, Lot No. 2800811) were purchased from Gibco (Thermo Fisher Scientific, Waltham, MA, USA). Penicillin−streptomycin solution (PS, Lot No. 240009024) was purchased from Sangon Biotech (Beijing) Co., Ltd., China. Cell counting Kit-8 (CCK-8, Lot No. ATXE21131) was purchased from GLPBIO (Montclair, CA, USA). 96-well plates (Cat. No. 3599) were purchased from Corning Incorporated (Corning, NY, USA).

2.2 Cell culture

HeLa human cervical adenocarcinoma cells were obtained from Wuhan Pusaite Biotechnology Co., Ltd., China. DMEM, FBS, and penicillin−streptomycin solution were purchased from Gibco. CCK-8 was obtained from Dojindo Molecular Technologies (Japan). HeLa cells were cultured in DMEM supplemented with 10% FBS and 1% penicillin−streptomycin at 37 °C in a humidified atmosphere containing 5% CO_2. Cells in logarithmic growth phase were used for all experiments.

2.3 Synthesis and characterization of KNMOH nanoflowers

KNMOH nanoflowers were synthesized via a two-step hydrothermal method. Briefly, manganese silicate precursors were treated with mixed KOH−NaOH solution (molar ratio of K to Na=2:1) at 90 °C for 12 h. The resulting product was washed, filtered, and dried to obtain $K_{0.37}Na_{0.18}MnO_2 \cdot 0.55H_2O$. The material was characterized by X-ray diffraction (XRD), scanning electron microscopy (SEM), and X-ray photoelectron spectroscopy (XPS) to confirm successful synthesis and structural integrity.

2.4 Cell viability assay

HeLa cells were seeded into 96-well plates at a density of 5×10^3 cells per well and incubated overnight to allow for cell attachment. Subsequently, the cells were treated with varying concentrations of KNMOH dispersed in complete culture medium for 24 h or 48 h. After the designated incubation period, 10 μL of Cell Counting Kit-8 (CCK-8) solution was added to each well. Following an additional 2 h incubation at 37 °C in the dark, the absorbance at 450 nm was measured using a microplate reader (BioTek Instruments, Winooski, VT, USA). The background absorbance from blank wells (medium with CCK-8 but without cells) was subtracted from all readings. Cell viability was calculated as a percentage relative to the untreated control group, which is A_t/A_c (A_t: absorbance of treated group; A_c: absorbance of control group).

2.5 Morphological observation

Cell morphological changes were observed using phase-contrast microscopy. HeLa cells were cultured in 6-well plates and treated with KNMOH at concentrations of 0, 50, and 100 μg/mL. Images were captured at 24 and 48 h post-treatment using an inverted microscope (Olympus CKX41, Japan).

2.6 Statistical analysis

Data are presented as the mean ± standard deviation (SD) from at least three independent experiments, with each experiment performed three times. Statistical significance was determined by one-way analysis of variance (ANOVA) followed by Dunnett's post hoc test using statistical software (GraphPad Prism, GraphPad Software, San Diego, CA, USA). A p-value <0.05 was considered statistically significant.

3 Results and discussion

3.1 Characteristic of KNMOH nanoflowers

The successful synthesis of KNMOH nanoflowers was confirmed through comprehensive characterization. XRD analysis (Fig. 1) reveals the characteristic peaks of δ-MnO_2 phase at 2θ=12.1°, 24.8°, and 37.2°, consistent with the layered structure reported in previous studies [14,16]. The incorporation of Na^+ and K^+ ions was evidenced by slight shifts in peak positions compared to pure δ-MnO_2, indicating successful doping without phase transformation [17].

To explore the elemental composition and valence state, XPS spectra of KNMOH nanoflowers are detected, as shown in Fig. 2. Figure 2(a) shows the survey spectra of Mn, O, Na, and K elements. In the original KNMOH nanoflowers, most Mn exists in the form of Mn^{4+}. The spectrum of O 1s is shown in Fig. 2(b) and the peaks of H—O—H, Mn—O—H and Mn—O—M are reflected at 532.9, 531.4 and 529.8 eV, respectively. In addition to bonding with Mn, some of O at the edge of the structure also bonds with H between layers or on the surface. The specific areas of Na 1s and K 2p are shown in Figs. 2(c, d), where the energy bands at 1071.1, 292.9, and 295.7 eV correspond to Na 1s, K $2p_{3/2}$, and K $2p_{1/2}$, respectively.

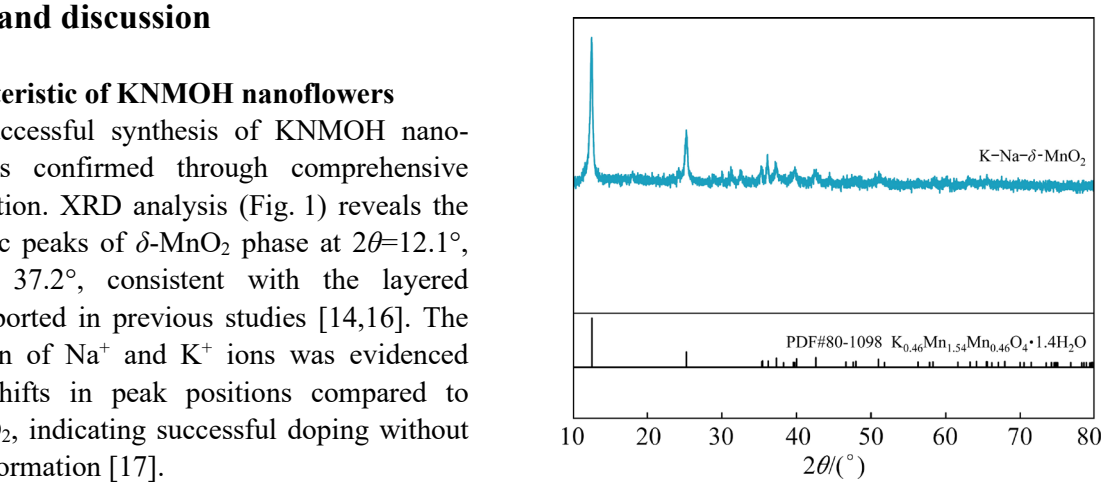

Fig. 1 XRD patterns of KNMOH nanoflowers (The characteristic peaks at 2θ=12.1°, 24.8°, and 37.2° correspond to the (001), (002), and (100) crystal planes of layered δ-MnO_2 structure, respectively)

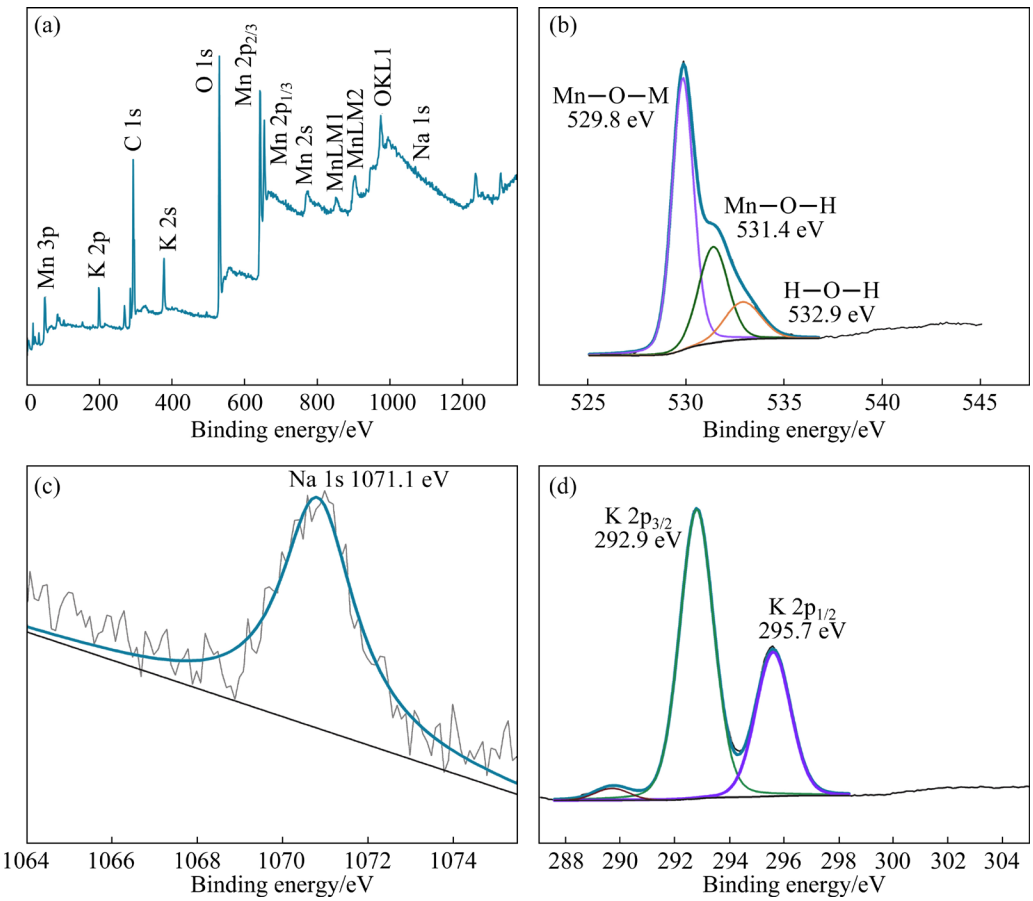

Fig. 2 XPS analysis of KNMOH nanoflowers: (a) Survey; (b) O 1s; (c) Na 1s; (d) K 2p

Figure 3 shows the microstructure of KNMOH. The flower-like morphology of the KNMOH composed of nanosheets is clearly observed from Fig. 3(a). In addition, the TEM image shows typical nanospheres with average diameter of 2−4 μm, composed of interconnected nanosheets with thickness of 20−30 nm (Fig. 3(b)). The HRTEM image clearly shows that the interlayer space of KNMOH is 0.71 nm in Fig. 3(c). This hierarchical morphology is crucial for enhancing surface area and improving cellular interaction [18,19]. Energy-dispersive X-ray spectroscopy (EDS) confirms the presence of K, Na, O and Mn elements with atomic ratios consistent with the target composition as shown in Fig. 3(d).

3.2 Dose-dependent cytotoxicity

The cytotoxic effects of KNMOH nanoflowers against HeLa cervical cancer cells were evaluated using the CCK-8 assay at concentrations of 50 and 100 μg/mL. As shown in Fig. 4, KNMOH nanoflowers demonstrated significant cytotoxicity at both tested concentrations. After 24 h of treatment, cell viability decreased to (36.8±6.5)% at 50 μg/mL and (33.4±6.4)% at 100 μg/mL (p<0.001).

After 48 h of treatment, cell viability was (45.2±2.3)% at 50 μg/mL and (32.3±2.8)% at 100 μg/mL. Interestingly, the concentration of 50 μg/mL showed a slight recovery in cell viability from 24 to 48 h (from 36.8% to 45.2%), while the concentration of 100 μg/mL maintained consistently low cell viability (from 33.4% to 32.3%). This suggests that the higher concentration (100 μg/mL) provides more sustained cytotoxic effects.

These results are compared with other MnO_2-based nanomaterials. For instance, HAO et al [20] demonstrated that MnO_2 nanosheets exhibited concentration-dependent cytotoxicity against various cancer cell lines, with half-maximal inhibitory concentration (IC_{50}) values ranging in 50−200 μg/mL. Similarly, FAN et al [21] reported that hollow MnO_2 nanoparticles showed significant cytotoxicity against HeLa cells at concentration above 25 μg/mL.

The cytotoxic mechanism of MnO_2-based materials is primarily attributed to their ability to catalyze the decomposition of intracellular H_2O_2, leading to the generation of reactive oxygen species (ROS) and subsequent oxidative stress [22]. The layered structure of δ-MnO_2 provides multiple active sites for such catalytic reactions, enhancing the cytotoxic efficacy [23,24].

The co-doping of Na and K ions in KNMOH nanoflowers may further enhance this cytotoxic activity through several mechanisms: (1) the expanded interlayer spacing (0.71 nm) facilitates

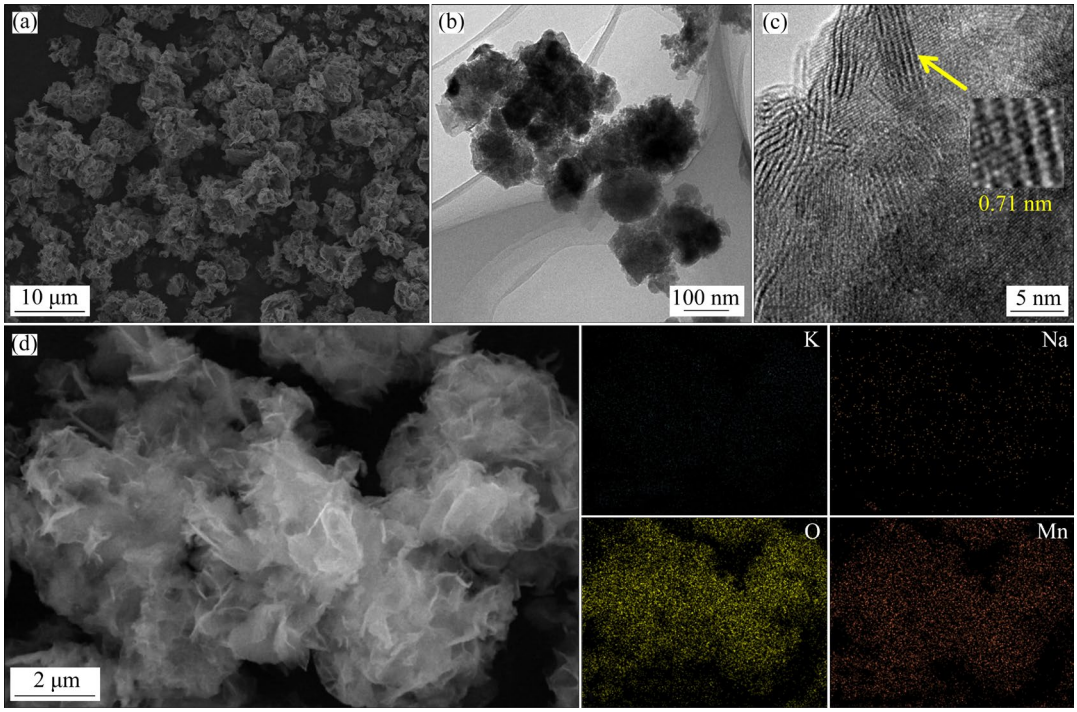

Fig. 3 Morphology and composition of KNMOH nanoflowers: (a) SEM image; (b) TEM image; (c) HRTEM image; (d) Elemental mapping

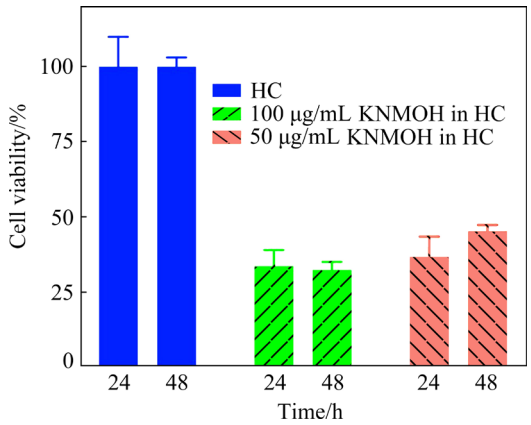

Fig. 4 Dose- and time-dependent cytotoxic effects of KNMOH nanoflowers on viability of HeLa cervical cancer cells (HC)

better cellular uptake and interaction with intracellular components; (2) the mixed alkali metal composition may create more defect sites that serve as catalytic centers for ROS generation; (3) the hierarchical nanoflower morphology provides a large surface-to-volume ratio, maximizing contact with cancer cells and enhancing the local concentration of reactive species at the cell−material interface. The unique structural features of KNMOH nanoflowers, including the expanded interlayer spacing and high surface area, may contribute to the enhanced cellular internalization through endocytic pathways, thereby increasing the intracellular concentration of the nanomaterial and amplifying its cytotoxic effects.

3.3 Time-dependent effects

At the concentration of 50 μg/mL KNMOH, there was an unexpected increase in cell viability from 36.8% at 24 h to 45.2% at 48 h. This phenomenon could be attributed to several factors: (1) potential cellular adaptation mechanisms, where surviving cells may upregulate antioxidant defense systems such as catalase and superoxide dismutase [25,26]; (2) depletion of reactive components over time due to consumption in catalytic reactions; (3) activation of cellular repair pathways that partially restore cellular function [27].

In contrast, at 100 μg/mL KNMOH, cell viability remained consistently low at both time (33.4% at 24 h vs 32.3% at 48 h), indicating sustained cytotoxic activity. This concentration appears to overcome cellular recovery mechanisms and maintains effective cytotoxic pressure over the extended treatment period. Similar observations have been reported for other nanomaterial-based therapies in Ref. [28], where higher concentrations can overwhelm cellular defense mechanisms.

The differential time-dependent responses suggest that KNMOH nanoflowers may have threshold-dependent mechanisms of action. Below a critical concentration threshold, cells retain capacity for adaptation through stress response pathways, while concentrations above this threshold induce irreversible cellular damage through overwhelming oxidative stress [29,30].

This biphasic response pattern has important implications for therapeutic dosing strategies. The partial recovery observed at 50 μg/mL KNMOH suggests that repeated dosing or continuous infusion protocols may be necessary to maintain therapeutic efficacy at low concentrations. Conversely, the sustained cytotoxicity at 100 μg/mL KNMOH indicates potential for the single-dose treatment regimen, though this must be balanced against potential systemic toxicity considerations. The threshold-dependent behavior may be related to the balance between ROS generation rate and cellular antioxidant capacity. At 50 μg/mL KNMOH, the initial burst of ROS may trigger cellular stress responses that temporarily overwhelm cellular defenses, but surviving cells can adapt by upregulating protective mechanisms. At 100 μg/mL KNMOH, the continuous and high-level ROS generation appears to exceed the cellular capacity for adaptation, leading to sustained cytotoxic effects.

3.4 Morphological analysis

Phase-contrast microscopy analysis reveals significant morphological changes of HeLa cells after KNMOH treatment (Fig. 5). Control cells exhibited typical adherent morphology with well-defined cellular boundaries and healthy cytoplasm. In contrast, treated cells showed characteristic features of cell death including cell shrinkage, membrane blebbing, cytoplasmic condensation, and detachment from the culture surface. These morphological changes are consistent with apoptotic cell death pathways, which have been previously associated with MnO_2-induced cytotoxicity [31,32]. The membrane blebbing and cell shrinkage observed are hallmarks of apoptosis, suggesting that KNMOH may trigger programmed cell death rather than necrotic pathways [33]. This

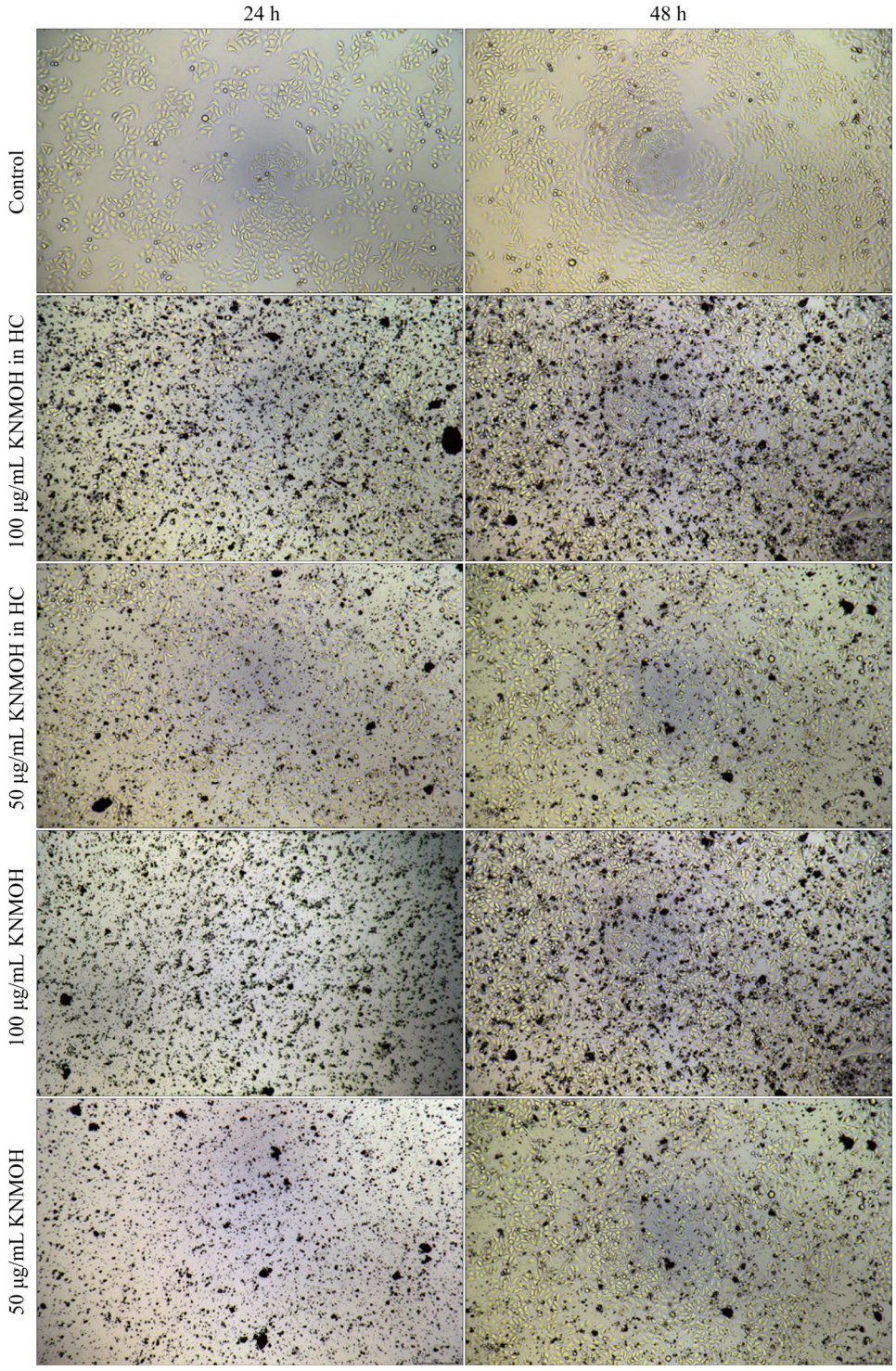

Fig. 5 Phase-contrast microscopy images showing morphological changes of HeLa cells after KNMOH treatment

is advantageous for potential therapeutic applications as apoptosis is generally associated with reduced inflammatory responses compared to necrosis [34].

The preferential induction of apoptosis by KNMOH could be attributed to the controlled release of ROS within the intracellular environment. The Mn^{4+}/Mn^{3+} redox cycling in the presence of cellular H_2O_2 generates a steady flux of ROS that activates intrinsic apoptotic pathways through mitochondrial dysfunction and caspase activation. The morphological changes, including membrane blebbing and nuclear condensation, are consistent with the activation of caspase-dependent apoptotic

pathways. Furthermore, the time-dependent progression of the morphological changes suggests an orderly apoptotic process rather than acute necrosis, which would typically result in rapid cell swelling and membrane rupture. Future mechanistic studies should focus on elucidating the specific apoptotic pathways activated by KNMOH, including analysis of caspase activation, mitochondrial membrane potential changes, and expression of pro- and anti-apoptotic proteins such as Bcl-2 family members.

4 Conclusions

(1) A two-step hydrothermal method yielded KNMOH nanoflowers with a well-defined birnessite-type layered structure. The successful incorporation of Na^+ and K^+ ions results in a significantly expanded interlayer spacing (approximately 0.71 nm). This expanded spacing, coupled with the nanoflower morphology, suggests enhanced surface area and potential for improved interactions with biological systems.

(2) The CCK-8 assay demonstrated a concentration- and time-dependent cytotoxic effect of KNMOH nanoflowers on HeLa cells. Higher concentrations and longer incubation periods resulted in significantly reduced cell viability.

(3) The observed cytotoxic effects, coupled with the controlled synthesis and unique structural features of KNMOH nanoflowers, suggest their potential as a novel anti-cancer agent.

CRediT authorship contribution statement

Qin CHEN: Conceptualization; Investigation, Cultivate cell, Cytotoxicity test, Writing – Original draft, Writing – Review and editing, Preparation; **Jin-quan YANG:** Cultivate cell, Writing – Review and editing, Supervision; **Jue LIU:** Investigation, Methodology.

Declaration of competing interest

The authors declare that they have no known competing financial interests or personal relationships that could have appeared to influence the work reported in this paper.

References

[1] BRAY F, LAVERSANNE M, SUNG H, FERLAY J, SIEGEL R L, SOERJOMATARAM I, JEMAL A. Global cancer statistics 2022: GLOBOCAN estimates of incidence and mortality worldwide for 36 cancers in 185 countries [J]. Cancer Journal for Clinicians, 2024, 74(3): 229−263.

[2] ABU-RUSTUM N R, YASHAR C M, AREND R, et al. NCCN guidelines® insights: Cervical cancer [J]. Journal of the National Comprehensive Cancer Network, 2023, 21(12): 1224−1233.

[3] RAI A, NOOR S, AHMAD S I, ALAJMI M F, HUSSAIN A, ABBAS H, HASAN G M. Recent advances and implication of bioengineered nanomaterials in cancer theranostics [J]. Medicina, 2021, 57(2): 91.

[4] BHATTACHARJEE B, KUPPUSAMY S, BISHWAS N R G, RYNJAH D, SAHU R K. Advanced smart nanomaterial-based system for treatment of cervical cancer: A systematic review [J]. Journal of Drug Delivery Science and Technology, 2024, 102(PA): 106327.

[5] FANG J F, WANG Q, YANG G J, XIAO X, LI L C, YU T. Albumin-MnO_2 gated hollow mesoporous silica nanosystem for modulating tumor hypoxia and synergetic therapy of cervical carcinoma [J]. Colloids and Surfaces B: Biointerfaces, 2019, 179: 250−259.

[6] WANG A T, WEN X, DUAN S Y, TIAN J W, LIU L, ZHANG W N. A gold cluster fused manganese dioxide nanocube loaded with dihydroartemisinin for effective cancer treatment via amplified oxidative stress [J]. RSC advances, 2024, 14(38): 27703−27711.

[7] GAO Yue, OUYANG Zhi-jun, SHEN Si-yan, YU Hong-wei, JIA Bing-yang, WANG Han, SHEN Ming-wu, SHI Xiang-yang. Manganese dioxide-entrapping dendrimers co-deliver protein and nucleotide for magnetic resonance imaging-guided chemodynamic/starvation/immune therapy of tumors [J]. ACS Nano, 2023, 17(23): 23889−23902.

[8] HAO Y W, ZHENG C X, WANG L, ZHANG J J, NIU X X, SONG Q L, FENG Q H, ZHAO H J, LI L, ZHANG H L, ZHANG Z Z, ZHANG Y. Tumor acidity-activatable manganese phosphate nanoplatform for amplification of photodynamic cancer therapy and magnetic resonance imaging [J]. Acta Biomaterialia, 2017, 62: 293−305.

[9] SONG G S, LIANG C, YI X, ZHAO Q, CHENG L, YANG K, LIU Z. Perfluorocarbon-loaded hollow Bi_2Se_3 nanoparticles for timely supply of oxygen under near-infrared light to enhance the radiotherapy of cancer [J]. Adv Mater, 2016, 28(14): 2716−2723.

[10] LIU Y, ZHEN W Y, JIN L H, ZHANG S T, SUN G Y, ZHANG T Q, XU X, SONG S Y, WANG Y H, LIU J H, ZHANG H J. All-in-one theranostic nanoagent with enhanced reactive oxygen species generation and modulating tumor microenvironment ability for effective tumor eradication [J]. ACS Nano, 2018, 12(5): 4886−4893.

[11] FAN W P, BU W B, SHEN B, HE Q J, CUI Z W, LIU Y Y, ZHENG X P, ZHAO K L, SHI J L. Intelligent MnO_2 nanosheets anchored with upconversion nanoprobes for concurrent pH-/H_2O_2-responsive UCL imaging and oxygen-elevated synergetic therapy [J]. Adv Mater, 2015, 27(28): 4155−4161.

[12] LIN L S, HUANG T, SONG J B, OU X Y, WANG Z T, DENG H Z, TIAN R, LIU Y J, WANG J F, LIU Y, YU G C, ZHOU Z J, WANG S, NIU G, YANG H H, CHEN X Y. Synthesis of copper peroxide nanodots for H_2O_2 self-supplying chemodynamic therapy [J]. J Am Chem Soc, 2019, 141(25): 9937−9945.

[13] ZHANG W, HU S L, YIN J J, HE W W, LU W, MA M, GU N, ZHANG Y. Prussian blue nanoparticles as multienzyme mimetics and reactive oxygen species scavengers [J]. J Am

Chem Soc, 2016, 138(18): 5860−5865.
[14] POST J E. Manganese oxide minerals: Crystal structures and economic and environmental significance [J]. Proceedings of the National Academy of Sciences of the United States of America, 1999, 96(7): 3447−3454.
[15] MASTERS J R. HeLa cells 50 years on: the good, the bad and the ugly [J]. Nature Reviews Cancer, 2002, 2(4): 315−319.
[16] UDDIN J, ABDUR R, HOSSAIN M R, AZIZ S, JAMAL M S, SHAIKH M A A, HOSSAIN M. Phase tunable nickel doped Mn_3O_4 nanoparticle synthesis by chemical precipitation: Kinetic study on dye degradation [J]. Nanoscale Advances, 2024, 6(3): 902−909.
[17] ZHANG K, HAN X P, HU Z, ZHANG X L, TAO Z L, CHEN J. Nanostructured Mn-based oxides for electrochemical energy storage and conversion [J]. Chem Soc Rev, 2015, 44(3): 699−728.
[18] WEI W F, CUI X W, CHEN W X, IVEY D G. Manganese oxide-based materials as electrochemical supercapacitor electrodes [J]. Chem Soc Rev, 2011, 40(3): 1697−1721.
[19] SUBRAMANIAN V, ZHU H W, VAJTAI R, AJAYAN P M, WEI B Q. Hydrothermal synthesis and pseudocapacitance properties of MnO_2 nanostructures [J]. J Phys Chem B, 2005, 109(43): 20207−20214.
[20] HAO R, XING R J, XU Z C, HOU Y L, GAO S, SUN S H. Synthesis, functionalization, and biomedical applications of multifunctional magnetic nanoparticles [J]. Adv Mater, 2010, 22(25): 2729−2742.
[21] FAN H M, YI J B, YANG Y, KHO K W, TAN H R, SHEN Z X, DING J, SUN X W, OLIVO M C, FENG Y P. Single-crystalline MFe_2O_4 nanotubes/nanorings synthesized by thermal transformation process for biological applications [J]. ACS Nano, 2009, 3(9): 2798−2808.
[22] YAO J, CHENG Y, ZHOU M, ZHAO S, LIN S C, WANG X Y, WU J, LI S R, WEI H. ROS scavenging Mn_3O_4 nanozymes for in vivo anti-inflammation [J]. Chem Sci, 2018, 9(11): 2927−2933.
[23] WANG W B, ZHAI W, CHEN Y, HE Q Y, ZHANG H. Two-dimensional material-based virus detection [J]. Sci China Chem, 2022, 65(3): 497−513.
[24] CHEN Z W, YIN J J, ZHOU Y T, ZHANG Y, SONG L N, SONG M J, HU S L, GU N. Dual enzyme-like activities of iron oxide nanoparticles and their implication for diminishing cytotoxicity [J]. ACS Nano, 2012, 6(5): 4001−4012.
[25] FORMAN H J, ZHANG H Q, RINNA A. Glutathione: Overview of its protective roles, measurement, and biosynthesis [J]. Mol Aspects Med, 2009, 30(1/2): 1−12.
[26] RAY P D, HUANG B W, TSUJI Y. Reactive oxygen species (ROS) homeostasis and redox regulation in cellular signaling [J]. Cell Signal, 2012, 24(5): 981−990.
[27] SCHIEBER M, CHANDEL N S. ROS function in redox signaling and oxidative stress [J]. Curr Biol, 2014, 24(10): R453−R462.
[28] NEL A, XIA T, MÄDLER L, LI N. Toxic potential of materials at the nanolevel [J]. Science, 2006, 311(5761): 622−627.
[29] LI N, XIA T, NEL A E. The role of oxidative stress in ambient particulate matter-induced lung diseases and its implications in the toxicity of engineered nanoparticles [J]. Free Radical Biol Med, 2008, 44(9): 1689−1699.
[30] XIA T, KOVOCHICH M, LIONG M, MÄDLER L, GILBERT B, SHI H B, YEH J I, ZINK J I, NEL A E. Comparison of the mechanism of toxicity of zinc oxide and cerium oxide nanoparticles based on dissolution and oxidative stress properties [J]. ACS Nano, 2008, 2(10): 2121−2134.
[31] YIN J J, LIU J, EHRENSHAFT M, ROBERTS J E, FU P P, MASON R P, ZHAO B Z. Phototoxicity of nano titanium dioxides in HaCaT keratinocytes: Generation of reactive oxygen species and cell damage [J]. Toxicol Appl Pharmacol, 2012, 263(1): 81−88.
[32] ZHANG Z, LIU F Y, CHEN J. Molecular structure of the ATP-bound, phosphorylated human CFTR [J]. Proceedings of the National Academy of Sciences of the United States of America, 2018, 115(50): 12757−12762.
[33] ELMORE S. Apoptosis: A review of programmed cell death [J]. Toxicol Pathol, 2007, 35(4): 495−516.
[34] ZAWADA W M, BANNINGER G P, THORNTON J, MARRIOTT B, CANTU D, RACHUBINSKI A L, DAS M, GRIFFIN W S T, JONES S M. Generation of reactive oxygen species in 1-methyl-4-phenylpyridinium (MPP+) treated dopaminergic neurons occurs as an NADPH oxidase-dependent two-wave cascade [J]. Journal of Neuroinflammation, 2011, 8: 129.

钾钠共掺杂层状二氧化锰 HeLa 细胞的毒性

陈 琴，杨进权，刘 珏

湖南省妇幼保健院，长沙 410008

摘 要：制备钾钠共掺杂 δ-MnO_2纳米花(KNMOH)，并评价其对 HeLa 宫颈癌细胞的毒性作用。研究结果表明，在 50 和 100 μg/mL 浓度下，KNMOH 表现出显著的剂量和时间依赖性细胞毒性。孵育处理 24 h 后，50 和 100 μg/mL 浓度下，细胞存活率分别降至(36.8±6.5)%和(33.4±6.4)%。延长处理时间至 48 h，相同浓度下的细胞存活率分别为(45.2±2.3)%和(32.3±2.8)%。相差显微镜观察显示，细胞出现特征性形态学改变，包括细胞皱缩和膜泡形成，表明细胞死亡。研究结果证实了 KNMOH 作为宫颈癌治疗药物的潜在应用价值，为深入探讨其作用机制奠定了基础。

关键词：钾钠共掺杂 δ-二氧化锰；细胞毒性；HeLa 细胞；层间距；宫颈癌

(Edited by Xiang-qun LI)